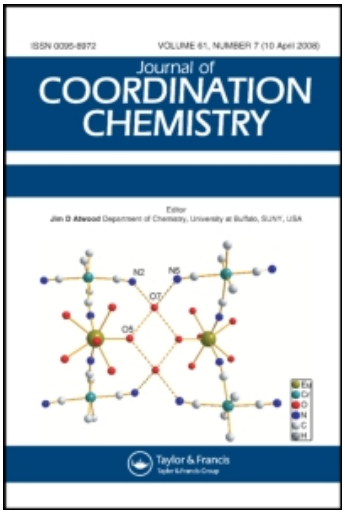

Journal of Coordination Chemistry
Publication details, including instructions for authors and subscription information:
http://www.informaworld.com/smpp/title~content=t713455674

A series of new hybrid compounds constructed from Dawson-type phosphomolybdates and metal-organic coordination complexes

Haiyan An[a]; Tieqi Xu[a]; Xuan Liu[a]; Cuiying Jia[a]
[a] Department of Chemistry, Dalian University of Technology, Dalian 116023, P.R. China

First published on: 04 August 2010

To cite this Article An, Haiyan , Xu, Tieqi , Liu, Xuan and Jia, Cuiying(2010) 'A series of new hybrid compounds constructed from Dawson-type phosphomolybdates and metal-organic coordination complexes', Journal of Coordination Chemistry, 63: 17, 3028 — 3041, First published on: 04 August 2010 (iFirst)
To link to this Article: DOI: 10.1080/00958972.2010.506215
URL: http://dx.doi.org/10.1080/00958972.2010.506215

Journal of Coordination Chemistry
Vol. 63, No. 17, 10 September 2010, 3028–3041

A series of new hybrid compounds constructed from Dawson-type phosphomolybdates and metal–organic coordination complexes

HAIYAN AN*, TIEQI XU, XUAN LIU and CUIYING JIA

Department of Chemistry, Dalian University of Technology, Dalian 116023, P.R. China

(*Received 9 October 2008; in final form 7 May 2010*)

In this study, a series of compounds based on Dawson-type phosphomolybdates, $H_3(C_6NO_2H_6)_2[K(H_2O)_3(C_6NO_2H_5)_3][P_2Mo_{18}O_{62}]\cdot 5.5H_2O$ (**1**), $(C_6NO_2H_6)_6[Ln(H_2O)_7(C_6NO_2H_5)_2]_2[P_2Mo_{18}O_{62}]_2\cdot 13.5H_2O$ (Ln = Ce (**2**), La (**3**)) have been synthesized and characterized by elemental analysis, IR and UV-Vis spectroscopy methods, TG analysis, and single-crystal X-ray diffraction. Compound **1** consists of $[P_2Mo_{18}O_{62}]^{6-}$ building units joined by potassium-pyridine-3-carboxylic acid complexes, resulting in a wavelike polyoxometalate (POM) chain, which further interacts with each other *via* intermolecular interactions to form a 3-D supramolecular channel framework containing guest water molecules. Compounds **2** and **3** possess a 3-D supramolecular framework with 1-D tunnel constructed from $[P_2Mo_{18}O_{62}]^{6-}$ and mononuclear lanthanide coordination complex fragments. To the best of our knowledge, **1** not only represents the first example of 1-D hybrid assembly based on Dawson-type phosphomolybdate, but also the first hybrid compound constructed from Dawson-type POMs and alkali–metal coordination complex fragments.

Keywords: Dawson-type phosphomolybdate; Alkali–metal coordination complex; Lanthanide coordination complex; 1-D chain; Supramolecular channel

1. Introduction

Polyoxometalates (POMs) [1–4] bear many properties that make them attractive for applications in catalysis, medicine, electrical, optical, and magnetic materials. An intriguing area in this field is the construction of hybrid materials based on POM building blocks and metal–organic coordination complexes due to the remarkable features of metal oxide surfaces and the diversities in the geometric topology [5–9]. Recently, Dawson-type phosphotungstate has attracted intensive interest, and some fascinating hybrid architectures based on it have been reported. For example, 1-D chains $[\{Ce(DMF)_4(H_2O)_3\}\{Ce(DMF)_4(H_2O)_4\}(P_2W_{18}O_{62})]\cdot H_2O$, $[\{La(DMF)_6(H_2O)\}\{La(DMF)_{4.5}(H_2O)_{2.5}\}(P_2W_{18}O_{62})]$ [10], and $H_{1.5}[Sm(H_2O)_8]_{0.5}[Sm(DMF)_6(H_2O)(P_2W_{18}O_{62})]\cdot DMF\cdot 3H_2O$ [11], 2-D layers $(NH_4)_3(H_2bipy)[Cu(bipy)]_7[P_2W_{18}O_{62}]_2\cdot 10H_2O$ [12] and $[4,4'\text{-}H_2bpy]_2\{[Cu(4,4'\text{-}bpy)_3][Cu(4,4'\text{-}bpy)_4(H_2O)_2]_2[Cu(4,4'\text{-}bpy)]$

*Corresponding author. Email: anhy@dlut.edu.cn

ISSN 0095-8972 print/ISSN 1029-0389 online © 2010 Taylor & Francis
DOI: 10.1080/00958972.2010.506215

$[\alpha\text{-}P_2W_{18}O_{62}]_2\} \cdot 6H_2O$ [13], 3-D frameworks $[Cu_6(btp)_3(P_2W_{18}O_{62})] \cdot 3H_2O$ (btp = 1,3-*bis*(1,2,4-triazol-1-yl)propane), $[Cu_6(btb)_3((P_2W_{18}O_{62})] \cdot 2H_2O$, $[Cu_3(btb)_6(P_2W_{18}O_{62})] \cdot 6H_2O$ (btb = 1,4-*bis*(1,2,4-triazol-1-yl)butane), $[Cu_3(btx)_{5.5}((P_2W_{18}O_{62})] \cdot 4H_2O$ (btx = 1,6-*bis*(1,2,4-triazol-1-yl)hexane) [14], $\{[Ag(bipy)]_2[P_2W_{18}O_{62}]\} \cdot 2[H_2bipy] \cdot 4H_2O$, $\{[Ag(bipy)]_4[P_2W_{18}O_{62}]\} \cdot 2[Hbipy]$, and $H_2[Ca_2(P_2W_{18}O_{62})(H_2O)_5] \cdot 7.5H_2O$ [15]. However, hybrid structures based on Dawson-type phosphomolybdate, especially extended architectures, remain largely unexplored, although they may possess potential use in electrocatalysis [16]. This is perhaps due to its relative low electron density on terminal and bridging oxygen atoms in contrast with the phosphotungstate. Therefore, the rational design and synthesis of hybrid architectures built up of Dawson-type phosphomolybdate cluster are of intense interest and a challenge in current synthetic chemistry.

Compared with a large number of the POM-based solid materials structurally modified by d-block [17] metal coordination complexes, s-block metal coordination subunits as linkers have been paid much less attention in assembling POM building blocks [18]. Potassium, with high biologic activity, is the primary cation in the cell sap, and it can adjust the penetrating press of the cells and the acid–base balance of body fluid. So far, only few examples of hybrid frameworks utilizing potassium coordination complexes as linkers were reported [19] due to their weak coordination ability. In addition, f-block metal coordination complexes have been extensively used as linkers to bridge different POM building blocks to yield hybrid species [20]; however, hybrid assemblies based on Dawson-type phosphomolybdate clusters and lanthanide coordination complexes have never been reported.

Herein, we choose pyridine-3-carboxylic acid as the organic component as a flexible ligand coordinating to various metal ions to give inorganic–organic hybrid materials [21]. In this article, we report three hybrid POMs, $H_3(C_6NO_2H_6)_2[K(H_2O)_3(C_6NO_2H_5)_3][P_2Mo_{18}O_{62}] \cdot 5.5H_2O$ (**1**), $(C_6NO_2H_6)_6[Ln(H_2O)_7(C_6NO_2H_5)_2]_2[P_2Mo_{18}O_{62}]_2 \cdot 13.5H_2O$ (Ln = Ce (**2**), La (**3**)) ($C_6NO_2H_5$ = pyridine-3-carboxylic acid). Compound **1** is built up of $[P_2Mo_{18}O_{62}]^{6-}$ clusters as the structural motif coordinatively linked by potassium-pyridine-3-carboxylic acid fragments to yield 1-D chains, which are further in close contact forming a 3-D supramolecular network. To the best of our knowledge, no analogous 1-D structure of Dawson-type phosphomolybdates and potassium coordination complex fragments has been reported. When Ce^{3+} and La^{3+} cations were used instead of K^+ cation, compounds **2** and **3** are obtained, possessing a 3-D supramolecular channel framework formed by hydrogen-bonding interactions between the Dawson-type $[P_2Mo_{18}O_{62}]^{6-}$ anions and mononuclear lanthanide coordination fragments. Additionally, the electrochemical properties of **1** and **2** have been studied.

2. Experimental

2.1. *General procedures*

All chemicals were commercially purchased and used without purification. $K_6[P_2Mo_{18}O_{62}] \cdot 14H_2O$ was synthesized according to the literature [22] and

characterized by IR spectrum. Elemental analyses (C, H, and N) were performed on a Perkin Elmer 2400 CHN elemental analyzer; P, Mo, La, Ce, and K were analyzed on a PLASMA-SPEC(I) ICP atomic emission spectrometer. IR spectra were recorded from 400 to 4000 cm^{-1} on an Alpha Centaurt FT-IR spectrophotometer using KBr pellets. UV-Vis spectra were obtained on a Unican UV-500 spectrometer (distilled water as solvent) in the range 900–190 nm. Thermal gravimetric (TG) analyses were performed on a Perkin Elmer TGA7 instrument in flowing N_2 with a heating rate of 10°C min^{-1}. A CHI 660 electrochemical workstation connected to a Digital-586 personal computer was used for control of the electrochemical measurements and for data collection. A conventional three-electrode cell contained glassy carbon as the working electrode, a saturated calomel electrode (SCE) as the reference electrode, and a platinum wire as the counter electrode.

2.2. *Preparation*

2.2.1. $H_3(C_6NO_2H_6)_2[K(H_2O)_3(C_6NO_2H_5)_3][P_2Mo_{18}O_{62}]\cdot 5.5H_2O$ (1). $K_6[P_2Mo_{18}O_{62}]\cdot 14H_2O$ (0.327 g, 0.1 mmol) was dissolved in 20 mL water. Pyridine-3-carboxylic acid (0.0592 g, 0.4 mmol) was added to the water solution. Then, 1 mol L^{-1} KCl (1 mL) was added. The mixture was heated for 1 h at 80°C after pH was adjusted to 3.5 with 1 mol L^{-1} NaOH. The filtrate was kept for 2 weeks at ambient conditions, and yellow block crystals of **1** were isolated in about 30% yield (based on Mo). Anal. Calcd for $H_3(C_6NO_2H_6)_2[K(H_2O)_3(C_6NO_2H_5)_3][P_2Mo_{18}O_{62}]\cdot 5.5H_2O$ (%): P, 1.72; Mo, 48.08; K, 1.09; C, 10.02; N, 1.95; and H, 1.31. Found (%): P, 1.93; Mo, 47.94; K, 1.33; C, 9.85; N, 1.71; and H, 1.48%. FT-IR data (cm^{-1}): 3441(vs), 2920(w), 2851(w), 1713(w), 1635(m), 1385(w), 1293(w), 1078(m), 1004(w), 939(s), 907(s), 838(s), 780(vs), 670(m), 526(m), and 452(w).

2.2.2. $(C_6NO_2H_6)_6[Ln(H_2O)_7(C_6NO_2H_5)_2]_2[P_2Mo_{18}O_{62}]_2\cdot 13.5H_2O$ (Ln = Ce (2), La (3)). In a typical procedure for **2**, $K_6[P_2Mo_{18}O_{62}]\cdot 14H_2O$ (0.327 g, 0.1 mmol) was dissolved in 20 mL water. Pyridine-3-carboxylic acid (0.0592 g, 0.4 mmol) was added to the solution and then $Ce(NO_3)_3\cdot 6H_2O$ (0.0868 g, 0.2 mmol) was added. The mixture was heated for 1 h at 80°C after pH was adjusted to 3.5 with 1 mol L^{-1} NaOH. The filtrate was kept for 3 weeks at ambient conditions, and yellow plate crystals of **2** were isolated in 34% yield (based on Mo). Anal. Calcd for $(C_6NO_2H_6)_6[Ce(H_2O)_7(C_6NO_2H_5)_2]_2[P_2Mo_{18}O_{62}]_2\cdot 13.5H_2O$ (%): P, 1.64; Mo, 45.60; Ce, 3.70; C, 9.51; N, 1.85; and H, 1.47. Found (%): P, 1.83; Mo, 45.30; Ce, 3.49; C, 9.33; N, 2.07; and H, 1.69. FT-IR data (cm^{-1}): 3444(vs), 1725(w), 1634(m), 1384(w), 1282(w), 1078(m), 1005(w), 939(s), 907(s), 831(s), 777(vs), 670(m), 507(m), and 453(w).

The preparation of **3** was similar to that of **2** except that $La(NO_3)_3\cdot 6H_2O$ was used instead of $Ce(NO_3)_3\cdot 6H_2O$. Crystals of **3** were obtained in 28% yield. Anal. Calcd for $(C_6NO_2H_6)_6[La(H_2O)_7(C_6NO_2H_5)_2]_2[P_2Mo_{18}O_{62}]_2\cdot 13.5H_2O$ (%): P, 1.64; Mo, 45.61; La, 3.67; C, 9.52; N, 1.85; and H, 1.47. Found (%): P, 1.85; Mo, 45.29; La, 3.56; C, 9.32; N, 1.99; H, 1.71. FT-IR data (cm^{-1}): 3425(vs), 2924(w), 2368(w), 1634(m), 1387(w), 1078(m), 939(s), 907(s), 834(s), 779(vs), 670(m), and 465(w).

Table 1. Crystal data and structure refinement for **1**–**3**.

Complex	**1**	**2**	**3**
Empirical formula	$C_{30}H_{47}KMo_{18}N_5O_{80.5}P_2$	$C_{60}H_{111}Ce_2Mo_{36}N_{10}O_{171.50}P_4$	$C_{60}H_{111}La_2Mo_{36}N_{10}O_{171.50}P_4$
Formula weight	3593.69	7574.55	7572.13
Temperature (K)	293(2)	293(2)	293(2)
Wavelength (Å)	0.71073	0.71073	0.71073
Crystal system	Monoclinic	Monoclinic	Monoclinic
Space group	$P2_1/c$	$P2_1/c$	$P2_1/c$
Unit cell dimensions (Å, °)			
a	14.0852(12)	13.805(3)	13.825(3)
b	21.716(2)	21.859(4)	21.870(4)
c	29.310(3)	29.839(6)	29.945(6)
α	90	90	90
β	101.401(5)	97.79(3)	97.95(3)
γ	90	90	90
Volume (Å^3), Z	8788.5(14), 4	8921(3), 2	8967(3), 2
Calculated density (g cm^{-3})	2.716	2.820	2.804
Absorption coefficient (mm^{-1})	2.683	3.102	3.055
Independent reflection	[R(int) = 0.0487]	[R(int) = 0.0552]	[R(int) = 0.1341]
Goodness-of-fit on F^2	1.044	1.058	1.034
Final R indices[a] [$I > 2\sigma(I)$]	$R_1 = 0.0468$, $wR_2 = 0.1227$	$R_1 = 0.0354$, $wR_2 = 0.0826$	$R_1 = 0.0754$, $wR_2 = 0.1440$
R indices (all data)	$R_1 = 0.0760$, $wR_2 = 0.1462$	$R_1 = 0.0487$, $wR_2 = 0.0899$	$R_1 = 0.1311$, $wR_2 = 0.1701$
Largest difference peak and hole (e Å^{-3})	1.846 and −0.994	1.464 and −0.913	2.574 and −1.429

[a] $R_1 = ||F_o| - |F_c||/|F_o|$; $wR_2 = [w(F_o^2 - F_c^2)^2]/[w(F_o^2)^2]^{1/2}$.

2.3. *X-ray crystallography*

Yellow single crystals with dimensions of $0.16 \times 0.14 \times 0.08\,mm^3$ for **1**, $0.17 \times 0.14 \times 0.09\,mm^3$ for **2**, and $0.15 \times 0.12 \times 0.08\,mm^3$ for **3** were fixed to the end of a glass capillary. The data were collected on a Bruker Smart-Apex CCD diffractometer with Mo-Kα (λ = 0.71073 Å) at 293 K for **1**. The data were collected on a Rigaku R-AXIS RAPID IP diffractometer with Mo-Kα (λ = 0.71073 Å) at 293 K for **2** and **3**. Empirical absorption corrections were also applied.

The structures of **1**–**3** were solved by direct methods and refined by full-matrix least-squares on F^2 using the *SHELXTL-97* software [23]. All non-hydrogen atoms in **1** were refined anisotropically. All the non-hydrogen atoms were refined anisotropically except for O1WA in **2** and OW9 in **3**. Hydrogens attached to carbon and nitrogen were fixed in ideal positions, and other hydrogens were not located. A summary of the crystallographic data and structural determinations for **1**–**3** is provided in table 1. Selected bond lengths and angles of **1** and **2** are listed in table 2.

3. Results and discussion

3.1. *Structure description*

3.1.1. Crystal structure of 1. Single-crystal X-ray analysis reveals that **1** is composed of $[P_2Mo_{18}O_{62}]^{6-}$ (abbreviated to P_2Mo_{18}) anionic clusters,

Table 2. Bond lengths (Å) and angles (°) with standard deviations in parentheses of **1** and **2**.

Compound **1**			
Mo(5)–O(7)	1.678(7)	K(1)–O(65)	2.674(1)
Mo(12)–O(10)	1.697(8)	K(1)–OW2	2.768(1)
Mo(16)–O(17)	1.685(7)	K(1)–OW1	2.84(2)
Mo(10)–O(61)	1.687(7)	K(1)–OW4	2.87(2)
Mo(7)–O(57)	1.758(6)	K(1)–O(17)	2.863(8)
Mo(7)–O(55)	2.155(7)	K(1)–O(67)	2.911(1)
Mo(4)–O(28)	2.299(7)	K(1)–O(61)$^{\#1}$	3.095(8)
Mo(16)–O(1)	2.395(7)	K(1)–O(63)	3.218(1)
Mo–O	1.678(7)–2.395(7)	P(1)–O(1)	1.573(7)
Mo–O_{av}	1.958	P(1)–O(12)	1.529(7)
O(20)–P(2)–O(59)	107.0(4)	O(12)–P(1)–O(21)	111.7(4)
Compound **2**			
P(1)–O(2)	1.531(4)	Ce(1)–O(65)	2.435(5)
P(1)–O(1)	1.577(4)	Ce(1)–O(63)	2.463(6)
Mo(18)–O(54)	1.825(5)	Ce(1)–O(1W)	2.468(13)
Mo(16)–O(54)	2.053(5)	Ce(1)–O(5W)	2.522(7)
Mo(6)–O(20)	1.802(4)	Ce(1)–O(7W)	2.552(6)
Mo(16)–O(50)	1.672(5)	Ce(1)–O(4W)	2.574(5)
Mo(7)–O(20)	2.037(4)	Ce(1)–O(2W)	2.588(6)
Mo(18)–O(33)	2.396(4)	Ce(1)–O(3W)	2.598(6)
Mo–O	1.531(4)–2.396(4)	Ce(1)–O(1WA)	2.600(10)
Mo–O_{av}	1.960	Ce(1)–O(6W)	2.654(5)
O(3)–P(1)–O(1)	107.5(2)	O(2)–P(1)–O(3)	111.9(2)

Symmetry transformations used to generate equivalent atoms in **1**: $^{\#1}$ x, $-y+3/2$, $z+1/2$.

potassium-pyridine-3-carboxylic acid subunits, isolated pyridine-3-carboxylic acid molecules, and free water. The Dawson P_2Mo_{18} structure may be described as two α-$[PMo_9O_{34}]^{9-}$ vacant anions, generated from the Keggin parent by the removal of three {MoOx} octahedra, and fused into a cluster of virtual D_{3h} symmetry (figure 1a). The structure may be described in terms of 12 equatorial Mo octahedra and 6 polar Mo octahedra. Four kinds of oxygen atoms exist in the cluster according to the manner of oxygen coordination, terminal oxygen (Ot), terminal oxygen linked to K^+ (Ot′), double-bridging oxygen (Ob), and central oxygen (Oc). Thus the Mo–O distances can be grouped into four sets: Mo–Ot 1.678–1.697 Å, Mo–Ot′ 1.685–1.687 Å, Mo–Ob 1.758–2.155 Å, and Mo–Oc 2.299–2.395 Å in **1**. The average Mo–O bond length is 1.958 Å. The central P–Oc distances vary from 1.529 to 1.573 Å. Bond angles of O–P–O range from 107.0° to 111.7°, indicating that {PO_4} tetrahedra are slightly distorted.

There is one crystallographically independent potassium. K(1) is eight-coordinate, in a distorted square antiprismatic coordination geometry, which is defined by two terminal oxygen atoms from two Dawson anions (K(1)–O = 2.863(8) and 3.095(8) Å), three oxygen atoms from three pyridine-3-carboxylic acid molecules (K(1)–O = 2.674(1), 2.911(1), and 3.218(1) Å), and three water molecules (K(1)–OW = 2.768(1), 2.840(2), and 2.870(2) Å). The average K(1)–O distance is 2.905 Å, which is close to K–O bond lengths in the literature [19, 24]. There are five crystallographically independent pyridine-3-carboxylic acid molecules adopting two kinds of different coordination modes. One kind of pyridine-3-carboxylic acid acts as a monodentate ligand by utilizing its carboxyl oxygen coordinating to K(1), and the other is the isolated protonated molecule.

The most remarkable feature in the structure of **1** is that the Dawson-type P_2Mo_{18} polyoxoanions are interlinked together *via* two potassium-pyridine-3-carboxylic acid

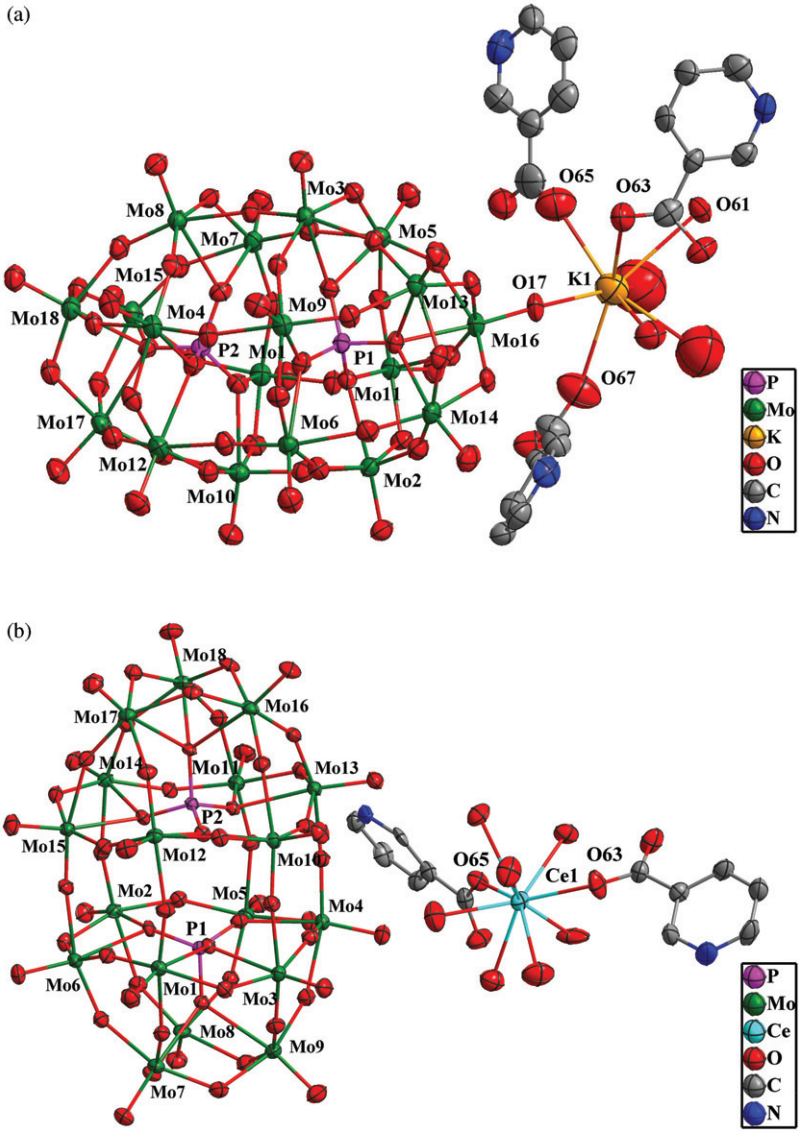

Figure 1. (a) ORTEP drawing of **1** with thermal ellipsoids at 50% probability. (b) ORTEP drawing of **2** with thermal ellipsoids at 50% probability. Free organic molecules and water molecules are omitted for clarity.

coordination complexes to generate an unusual chain (figure 2a). To the best of our knowledge, no analogous 1-D chain consisting of Dawson-type POM building blocks and potassium-organic complex units has been reported. These chains are linked to form a 2-D layer through strong hydrogen-bonding interactions between nitrogen atoms of pyridine-3-carboxylic acid and terminal oxygen atoms of polyoxoanions (N3 $\cdots$ O31 2.963 Å; figure 2b). Adjacent wavelike layers are supported by pyridine-3-carboxylic acid molecules to construct a 3-D supramolecular framework with 1-D channels *via* strong hydrogen-bonding interactions (N4 $\cdots$ O63 2.873, N3 $\cdots$ O69

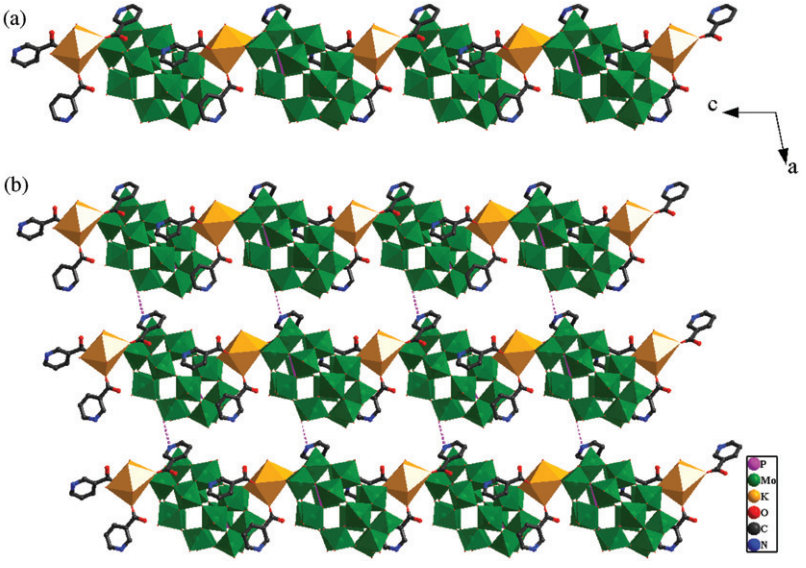

Figure 2. (a) Polyhedral and ball–stick view of the 1-D assembly wavelike chain in **1**. (b) Polyhedral and ball–stick view of the 2-D supramolecular layer in **1** along the *b*-axis (color code: P, purple; Mo, green; K, yellow; O, red; C, gray; and N, blue).

2.824 Å) between nitrogen atoms and oxygen atoms of pyridine-3-carboxylic acid (figure 3a). The dimensions of the channel are 9.7×6.5 Å along the *a* direction (figure 3b). Water and free organic molecules situate in the channels and form extensive hydrogen-bonding interactions with the host framework. The typical hydrogen bonds are OW6···O19 2.910, OW8···O25 2.898, N5···O34 2.908 Å. Extensive hydrogen-bonding interactions play an important role in stabilizing the 3-D supramolecular framework. By plenty of parallel experiments, we found that the choice of pyridine-3-carboxylic acid ligand was crucial. If we change pyridine-3-carboxylic acid to pyridine-4-carboxylic acid or other amino acid molecules, we cannot get potassium-organic subunit linked phosphomolybdates.

3.1.2. Crystal structures of 2 and 3. When we change metal cations from K^+ to Ce^{3+} and La^{3+}, we got **2** and **3**. The single-crystal X-ray diffraction analyses reveal that **1**–**3** are isostructural, the unit cell dimensions, volumes, related bond distances and angles are only slightly changed, and they all crystallize in the monoclinic space group $P2_1/c$. The metal cations have different coordination environments in compounds **2**(**3**) and **1** due to the small differences in metal cations; therefore, we discuss the structure of **2** in detail herein. The structure of **2** exhibits a 3-D supramolecular open framework composed of P_2Mo_{18} polyoxoanions, Ce-pyridine-3-carboxylic acid coordination complexes, isolated pyridine-3-carboxylic acid molecules, and free water. The P_2Mo_{18} cluster is a classic Dawson structure, with D_{3h} symmetry (figure 1b). Three kinds of oxygen exist in the cluster, terminal oxygen Ot, double-bridging oxygen Ob, and central oxygen Oc. Thus, the Mo–O distances can be grouped into three sets: Mo–Ot 1.672–1.802 Å, Mo–Ob 1.825–2.053 Å, and Mo–Oc 2.037–2.396 Å in **2**. The average Mo–O

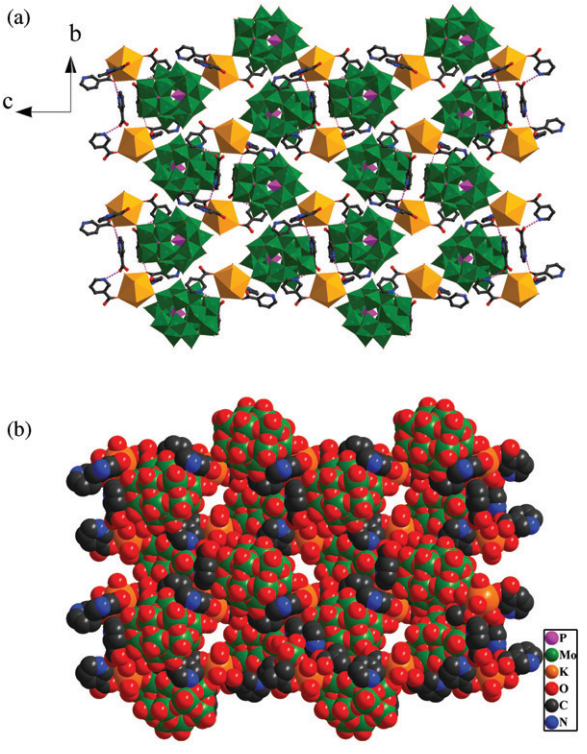

Figure 3. (a) Polyhedral and ball–stick view of the 3-D supramolecular framework of **1** along the *a*-axis showing the 1-D channels formed by weak interactions. (b) Space-filling diagram of the 3-D supramolecular channel framework of **1** (color code: P, purple; Mo, green; K, yellow; O, red; C, gray; and N, blue). Free water molecules are omitted for clarity.

bond length is 1.960 Å, which corresponds with that of **1**. The central P–Oc distances vary from 1.531 to 1.577 Å. The bond angles of O–P–O range from 107.5° to 111.9°, indicating that the $\{PO_4\}$ tetrahedra are slightly distorted.

There is one crystallographically independent Ce(1) which is nine-coordinate in a distorted tricapped trigonal prism defined by two oxygen atoms from two pyridine-3-carboxylic acids (Ce(1)–O = 2.435(5) and 2.463(6) Å) and seven water molecules (average Ce(1)–OW = 2.569 Å). The average Ce(1)–O distance is 2.545 Å, which is close to Ce–O bond lengths in the literature [20]. There are five crystallographically independent pyridine-3-carboxylic acid molecules adopting two different coordination modes. One kind of pyridine-3-carboxylic acid is a monodentate ligand by utilizing its carboxyl oxygen coordinating to Ce(1), the other is the isolated protonated molecule.

In the structure of **2**, the Dawson-type P_2Mo_{18} polyoxoanions are interlinked *via* two Ce-pyridine-3-carboxylic acid coordination complexes to generate a 1-D chain *via* strong hydrogen-bonding interactions O5W···O22 2.828, O6W···O55 2.839, and N2···O59 2.781 Å (figure 4a). Hydrogen bonds between coordinated water and Dawson polyoxoanions have been reported in $[Zn(phen)_2(ppy)][\{Zn(phen)_2\}\{Zn(phen)_2(H_2O)\}\{P_2W_{18}O_{62}\}]\cdot 2H_2O$ [25]. Then these chains are joined to yield a 2-D supramolecular layer *via* hydrogen-bonding interactions between free ligands

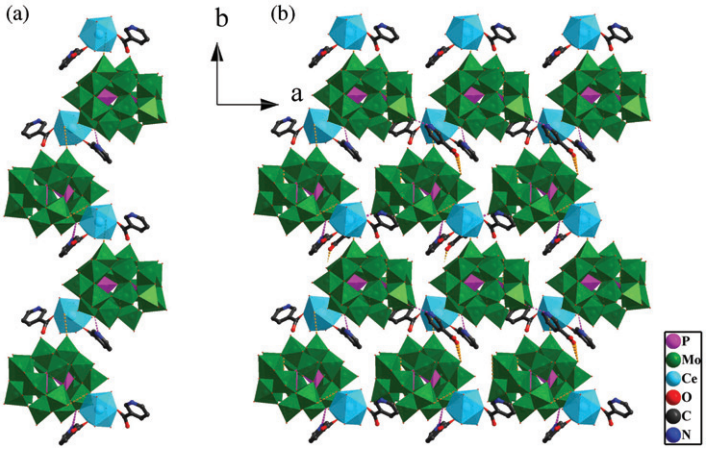

Figure 4. (a) Polyhedral and ball–stick view of the 1-D hydrogen-bonding chain in **2**. (b) View of the 2-D supramolecular layer in **2** along the *c*-axis (color code: P, purple; Mo, green; Ce, blue; O, red; C, gray; and N, blue).

and polyoxoanions (N3 · · · O9 2.920, O62 · · · O68 2.822 Å) (figure 4b). Adjacent layers are interconnected by cerium coordination complexes *via* strong hydrogen-bonding interactions between oxygen of P_2Mo_{18} polyoxoanions, and nitrogen of pyridine-3-carboxylic acid (O27 · · · N1 2.837 Å) to construct a 3-D supramolecular framework containing 1-D channels along the *a* direction; the dimensions of the channel are *ca* 7.6 × 6.2 Å (figure 5). Water molecules situate in the channels and form extensive hydrogen-bonding interactions with the host framework. Obviously, these strong hydrogen-bonding interactions play an important role in formation of the 3-D supramolecular framework.

Compounds **1**–**3** were obtained by conventional synthesis, differing from reported Dawson POM-based hybrid compounds that were mostly synthesized under hydrothermal condition [12–14, 25, 26]. The structures in **1**–**3** are all formed around Dawson-type P_2Mo_{18} clusters that play a fundamental role in the formation of the hybrid frameworks as precursors under the similar reaction condition. Compounds **1**–**3** are isostructural, and they all crystallize in the monoclinic space group $P2_1/c$. The slight structural difference between **1** and **2**(**3**) is due to alkali–metal and rare earth cations that have slightly different coordination geometry to result in the formation of slightly different supramolecular arrays. In **1**, K^+ has a distorted square antiprismatic coordination geometry and coordinates to terminal oxygen atoms of P_2Mo_{18}, whereas in **2** and **3**, Ln^{3+}, which does not coordinate to oxygen of P_2Mo_{18} polyoxoanions, has a distorted tricapped trigonal prism coordination environment and links to two organic ligands. Thus, metal cations can adjust the framework structure and properties.

The bond valence sum (BVS) calculations [27] indicate that P site is in the +5 oxidation state, all Mo sites are in the +6 oxidation state, K site is in the +1 oxidation state, and Ce and La sites are in the +3 oxidation state. According to the BVS values, the charge balance considerations, and weak acid reaction conditions in **1**, there are three protons which could not be located by the crystal structure analysis [28].

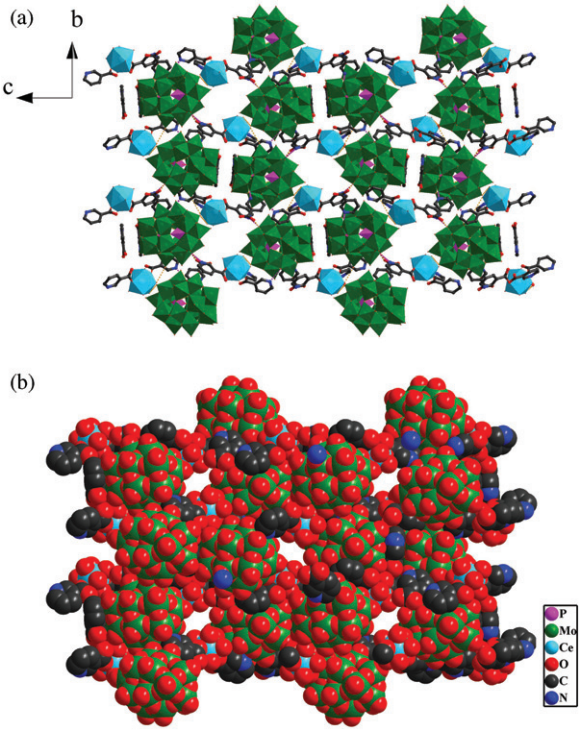

Figure 5. (a) Representation of the 3-D supramolecular framework of **2** along the *a*-axis showing the 1-D channels formed by weak interactions. (b) Space-filling diagram of the 3-D supramolecular channel framework of **2** (color code: P, purple; Mo, green; Ce, blue; O, red; C, gray; and N, blue). Free water molecules are omitted for clarity.

3.2. *FT-IR spectroscopy*

IR spectra of **1** exhibit the characteristic peaks of Dawson-type POMs and pyridine-3-carboxylic acid ligands (figure S2a). In the low-wave number regions of the IR spectra, they display the characteristic patterns of the Dawson structure [25, 29]. Also, **1** exhibits a band at 1078 cm^{-1} ascribed to ν(P–Oa), characteristic bands at 939 cm^{-1} attributed to ν(Mo–Ot), and 907 and 780 cm^{-1} attributed to ν(Mo–Oe/c–Mo) (Ot = terminal oxygen; Oe = bridged oxygen of two octahedral sharing an edge; and Oc = bridged oxygen of two octahedral sharing a corner). The compound shows characteristic bands of pyridine-3-carboxylic acid at 1713, 1635, 1385, and 1282 cm^{-1}. In the IR spectrum of **2** (figure S2b), characteristic peaks at 1078, 939, 907, and 777 cm^{-1} are attributed to the P_2Mo_{18} polyoxoanions. The features at 1725, 1634, 1384, and 1283 cm^{-1} in IR spectrum arise from pyridine-3-carboxylic acid molecules. The IR spectrum of **3** is similar to **2** (figure S2c).

3.3. *UV-Vis spectroscopy*

The UV spectrum (600–200 nm) of **1** in aqueous solution displays an intense absorption at 223 nm and a shoulder absorption centered at 323 nm (figure S3a). The higher

energy band can be assigned to Ot → Mo charge transfer, whereas the lower energy band is attributed to Ob(c) → Mo charge transitions in Dawson-type POMs [11, 30].

The UV spectrum of **2** in aqueous solution displays an intense absorption at 223 nm and a shoulder centered at 322 nm (figure S3b). The higher energy band can be assigned to Ot → Mo charge transfer and the lower energy band to Ob(c) → Mo. The UV spectrum of **3** in aqueous solution is similar to **2** (figure S3c).

3.4. *TG analysis*

TG curve of **1**, shown in figure S4(a), exhibits a three-step continuous weight loss and gives a total weight loss of 26.98% from 30°C to 600°C, which agrees with the calculated value of 26.57%. The weight loss at 30–600°C corresponds to the loss of all non-coordinated and coordinated water molecules, organic molecules and the sublimation of P_2O_5.

The TG curve of **2** exhibits three continuous weight loss stages from 40°C to 570°C (figure S4b), corresponding to the release of non-coordinated water, coordinated water, organic molecules, and sublimation of P_2O_5 molecules, respectively. The whole weight loss (25.62%) is in agreement with the calculated value (25.57%). The TG curve of **3** is similar to **2** (figure S4c).

3.5. *Electrochemical properties*

The electrochemical behaviors of **1** and **2** were investigated by cyclic voltammetry (CV). The cyclic voltammograms for **1** and **2** at different scan rates are presented in figure 6 in the potential range of +600 to −600 mV. There exists three reversible redox peaks I–I′, II–II′, and III–III′ with half-wave potentials $E_{1/2} = (E_{pa} + E_{pc})/2$ at 59 (I–I′), −98 (II–II′), and −310 (III–III′) mV (scan rate: 400 mV s^{-1}) in **1**, respectively. There also exists three reversible redox peaks I–I′, II–II′, and III–III′ with half-wave potentials at 62 (I–I′), −98 (II–II′), and −308 (III–III′) mV (scan rate: 400 mV s^{-1}) in **2**. The redox peaks I–I′, II–II′, and III–III′ correspond to three consecutive two-electron processes of the Mo centers in Dawson-type POMs [31].

When the scan rates were varied from 50 to 400 mV s^{-1} for **1** and **2**, the peak potentials change gradually with cathodic peak potentials shifting negative and the corresponding anodic peak potentials positive with increasing scan rates. The approximate proportionality of the reduction peak current to the scan rate up to 400 mV s^{-1} indicates that the redox process is surface-controlled. When the potential range is maintained between 600 and −600 mV, the peak currents remain almost unchanged after hundreds of cycles and with time, indicating that the compound is stable in aqueous solution.

4. Conclusion

Success in synthesizing isostructural compounds (**1**–**3**) provides examples of the utilities of pre-synthesized Dawson-type phosphomolybdate clusters as precursor, and s-block

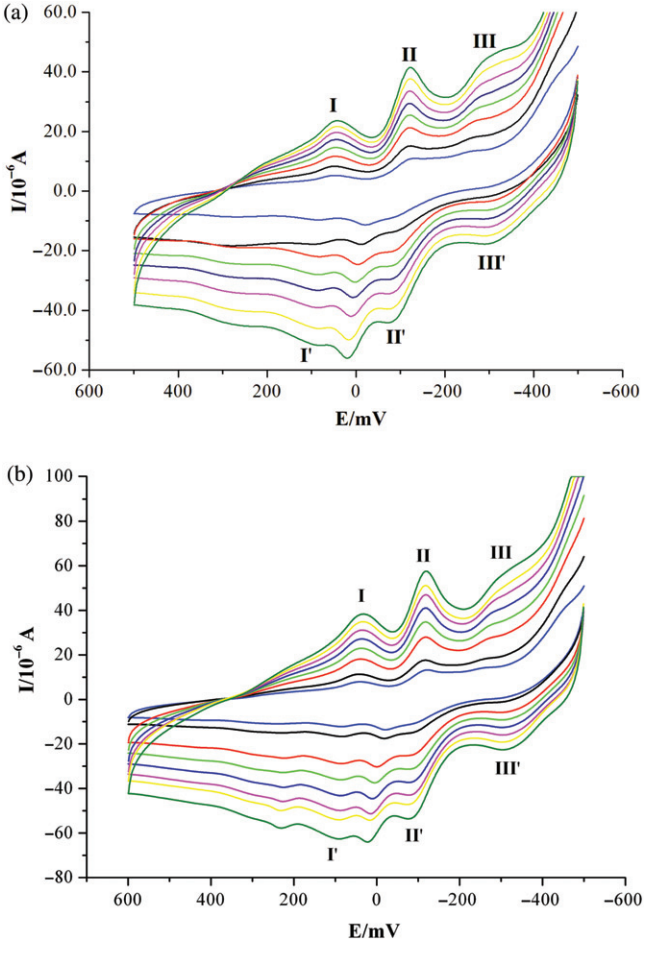

Figure 6. (a) Cyclic voltammograms of 4×10^{-4} mol L^{-1} **1** in the pH of 5 ($CH_3COONa + CH_3COOH$) buffer solution at different scan rates (from inner to outer: 50, 100, 150, 200, 250, 300, 350, and 400 mV s^{-1}). (b) Cyclic voltammograms of 4×10^{-4} mol L^{-1} **2** in the pH of 5 ($CH_3COONa + CH_3COOH$) buffer solution at different scan rates (from inner to outer: 50, 100, 150, 200, 250, 300, 350, and 400 mV s^{-1}).

and f-block metal coordination complexes as bridges for constructing hybrid architectures. The structure of **1** represents the first example of a 1-D chain composed of Dawson-type phosphomolybdates and potassium coordination fragments. The architecture of **1** exhibits a 3-D supramolecular channel framework *via* strong hydrogen-bonding interactions between pyridine-3-carboxylic acid molecules and polyoxoanions. Compounds **2** and **3** represent the first hybrid compound based on Dawson-type phosphomolybdates and lanthanide coordination complexes. In addition, the electrochemical properties of **1** and **2** may make candidates for potential electrocatalytic materials. This approach is expected to be effective for the further construction of other phosphomolybdate-based hybrid structures by selecting suitable second metals and organic ligands.

Supplementary material

The 3-D supramolecular framework of **3**, IR spectrum, TG curve, and UV-Vis spectrum for compounds **1**–**3** are available. CCDC reference nos 702188 for **1**, 756792 for **2**, and 756793 for **3**.

Acknowledgments

The authors thank the National Natural Science Foundation of China (20901013), Specialized Research Fund for the Doctoral Program of Higher Education (200801411012), and Scientific Research Foundation for Doctor of Liaoning Province of China (20081092) for providing financial support.

References

[1] M.T. Pope. *Heteropoly and Isopoly Oxometalates*, Springer, New York (1983).
[2] A. Müller, S.Q.N. Shah, H. Bögge, M. Schmidtmann. *Nature*, **397**, 48 (1999).
[3] P.J. Hagrman, D. Hagrman, J. Zubieta. *Angew. Chem. Int. Ed.*, **111**, 2798 (1999).
[4] K. Fukaya, T. Yamase. *Angew. Chem. Int. Ed.*, **42**, 654 (2003).
[5] D.L. Long, E. Burkhölder, L. Cronin. *Chem. Soc. Rev.*, **36**, 105 (2007).
[6] Y. Hou, X.K. Fang, C.L. Hill. *Chem. Eur. J.*, **13**, 9442 (2007).
[7] (a) M. Carraro, A. Sartorel, G. Scorrano, C. Maccato, M.H. Dickman, U. Kortz, M. Bonchio. *Angew. Chem. Int. Ed.*, **47**, 7275 (2008); (b) H.Y. An, Y.G. Li, E.B. Wang. *J. Coord. Chem.*, **59**, 379 (2006).
[8] (a) Y.Q. Lan, S.L. Li, Z.M. Su, K.Z. Shao, J.F. Ma, X.L. Wang, E.B. Wang. *Chem. Commun.*, 58 (2008); (b) Z.M. Zhang, Y.G. Li, E.B. Wang, X.L. Wang, C. Qin, H.Y. An. *Inorg. Chem.*, **45**, 4313 (2006).
[9] G.G. Gao, L. Xu, X.S. Qu, H. Liu, Y.Y. Yang. *Inorg. Chem.*, **47**, 3402 (2008).
[10] J.Y. Niu, D. Guo, J.P. Wang, J.W. Zhao. *Cryst. Growth Des.*, **4**, 241 (2004).
[11] J.P. Wang, J.W. Zhao, J.Y. Niu. *J. Mol. Struct.*, **697**, 191 (2004).
[12] H. Jin, Y.F. Qi, D.R. Xiao, X.L. Wang, S. Chang, E.B. Wang. *J. Mol. Struct.*, **837**, 23 (2007).
[13] J.W. Zhao, S.T. Zheng, W. Liu, G.Y. Yang. *J. Solid State Chem.*, **181**, 637 (2008).
[14] A.X. Tian, J. Ying, J. Peng, J.Q. Sha, Z.G. Han, J.F. Ma, Z.M. Su, N.H. Hu, H.Q. Jia. *Inorg. Chem.*, **47**, 3274 (2008).
[15] (a) J.Q. Sha, J. Peng, Y.Q. Lan, Z.M. Su, H.J. Pang, A.X. Tian, P.P. Zhang, M. Zhu. *Inorg. Chem.*, **47**, 5145 (2008); (b) J.P. Wang, D. Yang, J.Y. Niu. *J. Coord. Chem.*, **61**, 3651 (2008).
[16] (a) S. Himeno, M. Takamoto. *J. Electroanal. Chem.*, **492**, 63 (2000); (b) A.S.J. Wéry, J.M. Gutiérrez-Zorrilla, A. Luque, M. Ugalde, P. Romám. *Polyhedron*, **16**, 2589 (1997).
[17] H.Y. An, E.B. Wang, D.R. Xiao, Y.G. Li, Z.M. Su, L. Xu. *Angew. Chem. Int. Ed.*, **45**, 904 (2006).
[18] H.Y. An, D.R. Xiao, E.B. Wang, C.Y. Sun, Y.G. Li, L. Xu. *J. Mol. Struct.*, **751**, 184 (2005).
[19] J. Liu, Y.G. Li, E.B. Wang, D.R. Xiao, L.L. Fan, Z.M. Zhang, Y. Wang. *J. Mol. Struct.*, **837**, 237 (2007).
[20] P. Mialane, A. Dolbecq, F. Sécheresse. *Chem. Commun.*, 3477 (2006).
[21] H.Y. An, Y.G. Li, E.B. Wang, D.R. Xiao, C.Y. Sun, L. Xu. *Inorg. Chem.*, **44**, 6062 (2005).
[22] H. Wu. *J. Biol. Chem.*, **43**, 189 (1920).
[23] (a) G.M. Sheldrick. *SHELXL-97, Program for Crystal Structure Refinement*, University of Gőttingen, Germany (1997); (b) G.M. Sheldrick. *SHELXL-97, Program for Crystal Structure Solution*, University of Gőttingen, Germany (1997).
[24] (a) E. Coronado, C. Giménez-Saiz, C.J. Gómez-García, S.C. Capelli. *Angew. Chem. Int. Ed.*, **43**, 3022 (2004); (b) S. Chang, C. Qin, E.B. Wang, Y.G. Li, X.L. Wang. *Inorg. Chem. Commun.*, **9**, 727 (2006).
[25] (a) A.X. Tian, Z.G. Han, J. Peng, J.L. Zhai, B.X. Dong, J.Q. Sha. *J. Coord. Chem.*, **60**, 1645 (2007); (b) J.F. Gaevey, M.T. Pope. *Inorg. Chem.*, **17**, 1115 (1978).
[26] (a) F. Yao, F.X. Meng, Y.G. Chen, C.J. Zhang. *J. Coord. Chem.*, **63**, 196 (2010); (b) Y.K. Lu, X.B. Cui, J.N. Xu, Q. Gao, Y. Chen, J. Jin, S.Y. Shi, J.Q. Xu, T.G. Wang. *J. Coord. Chem.*, **63**, 394 (2010).
[27] I.D. Brown, D. Altermatt. *Acta Crystallogr.*, **B41**, 244 (1985).

[28] N. Honma, K. Kusaka, T. Ozeki. *Chem. Commun*., 2896 (2002).
[29] L.E. Briand, G.M. Valle, H.J. Thomas. *J. Mater. Chem*., **12**, 299 (2002).
[30] J.S. Zhang, L. Xua, Y. Cui, W.X. Cao, Z. Li. *Mater. Chem. Phys*., **90**, 47 (2005).
[31] (a) E. Papaconstantinou, M.T. Pope. *Inorg. Chem*., **6**, 1152 (1967); (b) B. Keita, L. Nadjo, R. Contant. *J. Electroanal. Chem*., **443**, 168 (1998); (c) A.M. Bond, T. Vu, A.G. Wedd. *J. Electroanal. Chem*., **494**, 96 (2000).